IEEE Access
Multidisciplinary | Rapid Review | Open Access Journal

Received 20 April 2023, accepted 1 May 2023, date of publication 11 May 2023, date of current version 6 June 2023.

*Digital Object Identifier 10.1109/ACCESS.2023.3275444*

RESEARCH ARTICLE

# Design and Optimization of Axial Field Flux-Switching Magnetic Gear Composite Motor Based on Varying-Network Magnetic Circuit

**XIAOBIN XU, WEI ZHANG, (Member, IEEE), JINRU CHENG, JIANWEI ZHAO, AND FENG QIAN**

School of Electrical Engineering, Nantong University, Nantong, Jiangsu 226019, China

Corresponding author: Wei Zhang (zhang.w@ntu.edu.cn)

This work was supported by the Natural Science Foundation of Jiangsu Province (NSFJP) under Grant BK20211332.

**ABSTRACT** Axial field flux-switching magnetic gear composite motor (AFFSMGCM) combines the advantages of axial field flux-switching permanent magnet machine (AFFSPMM) and magnetic gear (MG). In order to reduce the time and cost of design and optimization due to the complicated structure of AFFSMGCM, the nonlinear varying-network magnetic circuit (VNMC) is researched and developed for the machine. First, the topology of AFFSMGCM is introduced in details. Then, the accurate VNMC model is established with consideration of magnetic saturation and leakage flux. Finally, multi-objective optimization of AFFSMGCM based on VNMC is carried out to obtain large torque and low torque ripple. Meanwhile, the finite element analysis (FEA) method is used to validate the VNMC model. It is shown that the calculation results based on VNMC model are similar to those of FEA. The proposed VNMC improves the efficiency and accuracy of the design and optimization of the machine.

**INDEX TERMS** Axial field flux-switching magnetic gear composite machine (AFFSMGCM), varying-network magnetic circuit (VNMC), sensitivity analysis, multi-objective optimization, finite element analysis (FEA) method.

## NOMENCLATURE

| | |
|---|---|
| $l_s$ | axial length of stator |
| $l_{st}$, $l_{sy}$ | axial length of stator teeth and yoke |
| $l_{rt}$, $l_{mry}$ | axial length of RMMR teeth and yoke |
| $l_{ry}$, $l_{rpm}$ | axial length of PM rotor yoke and rotor PM |
| $w_s$ | width of E-typed stator core |
| $w_{st}$, $w_{smt}$ | width of stator side tooth and middle tooth |
| $w_{mry}$, $w_{rt}$ | width of RMMR yoke and tooth |
| $w_{sl}$ | width of stator slot |
| $w_{spm}$, $w_{rpm}$ | width of stator PM and rotor PM |
| $g_1$ | length of inner air gap |
| $g_2$ | length of outer air gap |
| $R_{sy}$ | reluctance of stator yoke |
| $R_{st}$, $R_{smt}$ | reluctance of stator side tooth and middle tooth |
| $R_{mry}$ | reluctance of RMMR yoke |
| $R_{rt}$ | reluctance of RMMR tooth |
| $R_{lt}$, $R_{ls}$ | reluctance of flux leakage between stator teeth and reluctance of flux leakage in stator slots |
| $R_{sl}$, $R_{ml}$ | reluctance of the internal and external magnetic leakage at the end of the stator PM |

The associate editor coordinating the review of this manuscript and approving it for publication was Philip Pong.

## I. INTRODUCTION

In recent years, the environmental pollution and energy crisis have become increasingly serious, and the concept of green travel has been deeply rooted in the hearts of the people. Electric vehicles and electric bicycles are becoming more and more popular. Therefore, the research and development of high efficiency and lightweight motors has important significance for the development of the electric vehicle industry [1], [2], [3].

This work is licensed under a Creative Commons Attribution-NonCommercial-NoDerivatives 4.0 License.
For more information, see https://creativecommons.org/licenses/by-nc-nd/4.0/

Axial field flux-switching magnetic gear composite motor (AFFSMGCM) combines the advantages of axial field flux-switching permanent magnet machine (AFFSPMM) and magnetic gear (MG). It can not only provide low speed and large torque in limited space, but also avoid the problems of noise, vibration, lubrication and cooling caused by mechanical gear reducer, thus deducing the maintenance costs and enhance the system reliability. Therefore, it has great application prospects in wind power, electric vehicles, ships and other fields [4], [5].

In the process of motor design and optimization, the finite element analysis (FEA) method has become the most common method of motor magnetic field analysis with the advantages of convenient use, high accuracy and strong versatility [6], [7], [8]. However, due to the complex structure and various parameters of AFFSMGCM, it is necessary to frequently adjust the parameters and establish a three-dimensional FEA model to calculate electromagnetic field at the early stage of the design, which increases time consumption and leads to low design efficiency. The analytical method can effectively analyze the influence of parameter changes on the electromagnetic performance, but it cannot be applied to complex boundary conditions, which may result in lower calculation accuracy than FEA method [9]. The lumped-parameter magnetic equivalent circuit method can improve the calculation accuracy and speed of motors, but it is not suitable for complex motor structures and is often used to establish the equivalent thermal network of motors [10].

The nonlinear VNMC method has the advantages of simple, fast calculation speed and high accuracy, and is often used in the initial design, performance analysis and parameter optimization of various types of motors [11], [12], [13], [14], [15]. Reference [12] used this method to analyze the driving characteristics of flux-switching permanent-magnet machines, and effectively considered the influence of end flux leakage. Reference [13] improved the magnetic network on the basis of the conventional VNMC model by introducing saturation coefficients, which effectively corrected and improved the calculation accuracy of the motor characteristic parameters.

However, due to the complex structure of AFFSMGCM and the existence of two groups of rotating parts, it is a challenging to the above mentioned VNMC models to provide the fast calculation and the precise design for the machine.

In the process of motor design and optimization, due to the conflicts between design parameters on different performance indicators, single-objective optimization methods can not meet the practical optimization needs, so scholars have developed and applied different optimization algorithms to multi-parameter and multi-objective optimization of motors [16], [17], [18], [19], [20], [21]. References [16] and [17] used a sequential Taguchi method to optimize a permanent magnet synchronous motor (PMSM). Although the method largely improved the efficiency of optimization, the design accuracy is sacrificed. In [18], a continuous ant colony algorithm was adopted to a high-speed surface-mounted PMSM to obtain the maximum output torque, but the parameter setting of the algorithm was determined by experimental method, leading to the empirical error. Reference [19] proposed a multi-objective large-scale design optimization method based on the FEA method and combined multi-objective optimization with the differential evolution (CMODE) algorithm for the parameter search process of optimization. Although using the FEA model for multi-objective optimization of motors can improve accuracy, the calculation of complex FEA models consumes a lot of time. Xiaoyong et al. combined the design of experience (DOE) with the response surface (RS) method to optimize a linear motor in order to increase the torque, improve the demagnetization ability, and reduce the torque ripple, which effectively improved the optimal accuracy. Although this method may lead to the extreme phenomenon of colony loss and reduce the efficiency of optimization, the authors adopted a simple magnetic equivalent circuit (MEC) model to calculate the torque, thereby reducing the overall optimization time [20]. In [21], a fast multi-objective analytical design for a spoke-type PM motor with Auxiliary Notches structure was proposed based on lumped-parameter MEC and a hybrid multi-objective optimizer. It was found that the results of optimal designs calculated by MEC model match well with the FEA model and prototype experimental results. The VNMC method is developed from the MEC method and can also be used for motor optimization. Reference [15] adopted the VNMC model for multi-objective optimization of a PM flux-switching motor, ensuring calculation accuracy while also reducing the optimization time. AFFSMGCM has the coupling problem between AFFSPMM and MG optimization. The complex influence between different design parameters need to be considered. Therefore, how to use VNMC method to accurately and efficiently optimize AFFSMGCM with multi-parameter and multi-objective is an important but challenging problem.

In this paper, the nonlinear VNMC model of AFFSMGCM is proposed for fast calculation and accurate analysis of the electromagnetic performance in the early design stage of the motor. In addition, the BP neural network algorithm and cuckoo algorithm are combined for multi-objective optimization of the motor based on the proposed VNMC model to obtain the large torque and low torque ripple. The AFFSMGCM topology is studied in section II. The accurate VNMC model is established in section III to calculate the electromagnetic characteristics. After sensitivity analysis of AFFSMGCM's structural parameters based on VNMC method, the high-level sensitivity parameters are multi-optimized by BP algorithm and Cuckoo algorithm in section IV. Finally, the conclusions are given in Section V.

## II. TOPOLOGY OF AFFSMGCM

Figure 1 shows the three-dimensional topology of an AFFSMGCM. The main design parameters of the motor are shown

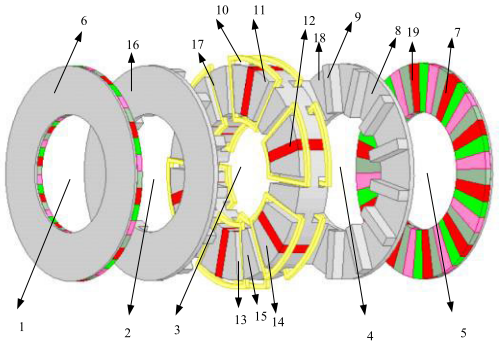


**FIGURE 1.** 3-Dimensional topology of AFFSMGCM. 1-PM rotor 1, 2-RMMR 1, 3-stator, 4-RMMR 2, 5-PM rotor 2, 6-PM rotor yoke, 7-rotor PM, 8-RMMR yoke, 9-RMMR tooth, 10-armature winding, 11-stator core, 12-stator PM, 13-stator slot, 14-stator side tooth, 15-stator middle tooth, 16-outer air gap 1, 17-inner air gap 1, 18-inner air gap 2, 19-outer air gap 2.

**TABLE 1.** Initial parameters of affsmgcm.

| Parameters(unit) | Values |
|---|---|
| Rated power (W) | 800 |
| Rated speed (rpm) | 975 |
| Pole pairs of stator PM | 3 |
| Pole pairs of rotor PM | 10 |
| Pole number of the RMMR | 13 |
| Transmission ratio | 1.3 |
| Axial length of stator (mm) | 40 |
| Stator PM inner arc width (°) | 10 |
| Stator tooth inner arc width (°) | 10 |
| Stator slot inner arc width (°) | 10 |
| Axial length of RMMR (mm) | 20 |
| RMMR tooth inner arc width (°) | 10.5 |
| Rotor PM inner arc width (°) | 8 |
| Axial length of PM rotor (mm) | 10 |
| Axial length of inner and outer air gap (mm) | 1 |
| Inner diameter of stator/rotor (mm) | 132 |
| Outer diameter of stator/rotor (mm) | 240 |

in Table 1. As shown in Figure 1, the AFFSMGCM is composed of the AFFSPMM and the MG, including one stator, two rotary magnetic modulation rings (RMMRs), and two PM rotors. It contains two groups of air gaps, the air gap between the stator and the RMMR is defined as the inner air gap, and the air gap between the RMMR and the PM rotor is defined as the outer air gap. The stator consists of 6 double E-typed stator cores, 6 PMs and 12 armature winding coils. The double E-typed stator cores and PMs are alternately placed to form a stator disc, PMs are alternately magnetized along the circumferential direction. The armature winding coils are wound around the two adjacent stator side teeth.

A single RMMR has 13 teeth evenly distributed on the yoke. The rotor PMs adopt Halbach array to enhance the magnetic density of outer air gap and reduce the harmonic of the magnetic flux density. Based on the magnetic regulation mechanism, the magnetic field of the stator and the rotor are coupled through RMMR, which can reduce the torque ripple and widen the speed regulation range while achieving the torque transmission.

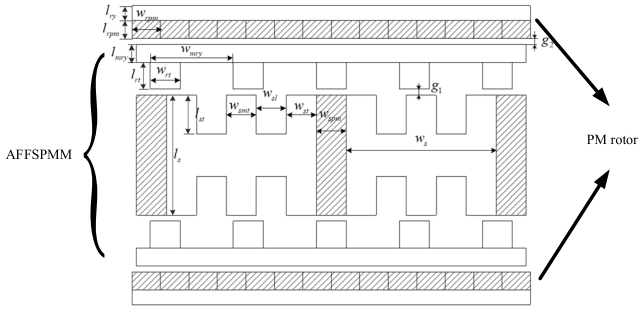


**FIGURE 2.** 2-Dimensional equivalent expansion view of AFFSMGCM.

## III. ESTABLISH AND VALIDATION OF VNMC

### A. MAGNETIC FIELD DISTRIBUTION OF AFFSMGCM

As Figure 1 shown, the AFFSMGCM can be equivalent to the parallel connection of two sub-motors composed of 1/2 stator, a RMMR and a PM rotor. The main parameters of the AFFSMGCM are shown in Figure 2. It can be seen from Figure 3 that the magnetic field distribution of the two sub-motors are the same. Therefore, a half of AFFSMGCM is used to build VNMC model for easy calculation.

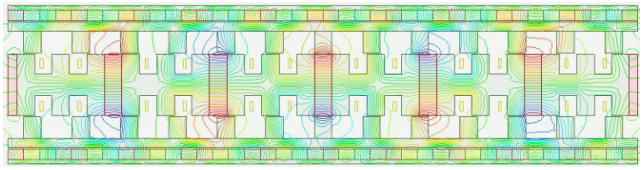

**FIGURE 3.** Magnetic field distribution in expansion view of AFFSMGCM.

### B. EQUIVALENT MAGNETIC CIRCUIT MODEL OF AFFSPMM

Since the stator of the motor is composed of 6 modular stator cores and 6 PMs, 1/6 equivalent magnetic circuit of AFFSPMM is acted as an example to introduced in Figure 4 and Figure 5. The PM magnetic field of stator and rotor and exist in the RMMR yoke at the same time, in order to improve the calculation accuracy, the magnetic circuit of the yoke is divided into two layers according to the axial direction, as shown in Figure 5.

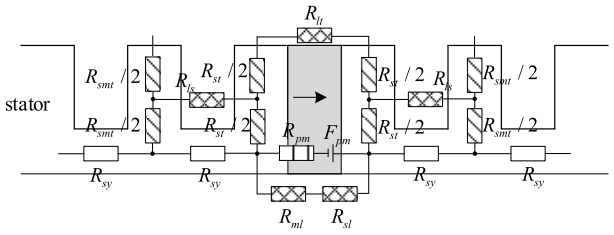


**FIGURE 4.** Equivalent magnetic circuit of the stator.

Considering the influence of magnetic saturation, $R_{sy}$, $R_{st}$, $R_{smt}$, $R_{mry}$, and $R_{rt}$ adopt nonlinear reluctance. $R_{lt}$, $R_{ls}$, $R_{sl}$ and $R_{ml}$ are represented by linear reluctance respectively. The PMs are equivalent to the magnetomotive force source

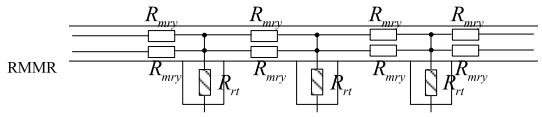


**FIGURE 5.** Equivalent magnetic circuit of RMMR.

$F_{pm}$ and the internal magnetic reluctance $R_{pm}$ and the calculation formula of $F_{pm}$ and $R_{pm}$ are as follows:

$$F_{pm} = \frac{B_r h_m}{\mu_0 \mu_r} \tag{1}$$

$$R_{pm} = \frac{h_m}{\mu_0 \mu_r l_m l_e} \tag{2}$$

where, $B_r$ is the remanence of PMs, $h_m$ and $l_m$ are the thickness in magnetization direction and height of the PMs, $\mu_0, \mu_r$ respectively are vacuum permeability and relative permeability of PMs, $l_e$ is the radial effective length, $l_e = (D_{so} - D_{si})/2, D_{so}, D_{si}$ are the inner and outer diameter of the stator.

It can be found in Figure 3 that there is a coupling magnetic field at the yoke of RMMR, so it is divided into two layers in the axial direction to improve calculation accuracy as the Figure5 shown.

According to the magnetic field distribution of AFFSPMM's iron cores in Figure 3, the magnetic field is mainly divided into circumferential magnetic field in yoke and axial magnetic field in teeth. The equivalent flux tubes in iron core of AFFSPMM are indicated in Figure 6. According to Figure 6, the reluctance of the stator yokes and the RMMR yokes adopt circumferential equivalent flux tube $R_c$, the stator teeth and RMMR teeth adopt axial equivalent flux tube $R_a$. The $R_c$ and $R_a$ can be calculated by (3)-(4).

$$R_c = \frac{\theta}{\mu l \ln(\frac{r_1}{r_2})} \tag{3}$$

$$R_a = \frac{l}{\mu w l_e} \tag{4}$$

where, $\mu$ is the core permeability, $\theta$ is radian; $l$ and $w$ are the dimensions shown in Figure 6(b).

Magnetic leakage flux can be divided into two types as shown in Figure 7 according to the shape, and the corresponding calculation formula is expressed in (5) and (6), respectively.

$$R_{la} = \frac{1}{0.26\mu_0 l_e} \tag{5}$$

$$R_{lb} = \frac{\pi}{\mu_0 l_e \ln\left(\frac{X_1+2t}{X_1}\right)} \tag{6}$$

where, $X_1$ and $t$ are the dimensions shown in Figure 7(b).

### C. EQUIVALENT MAGNETIC CIRCUIT MODEL OF PERMANENT MAGNET ROTOR

Since the rotor PMs adopt Halbach array, the magnetic circuits of circumferentially and axially magnetized PMs

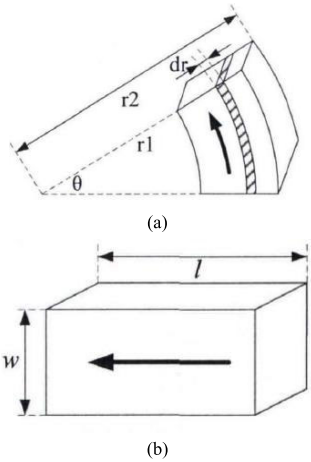


**FIGURE 6.** Equivalent flux tube in iron core of AFFSPMM. (a) circumferential magnetic field. (b) axial magnetic field.

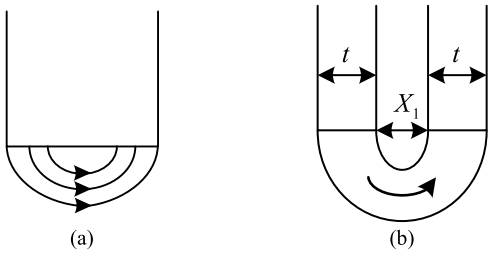


**FIGURE 7.** Type of leakage flux path. (a) leakage flux of type 1. (b) leakage flux of type.

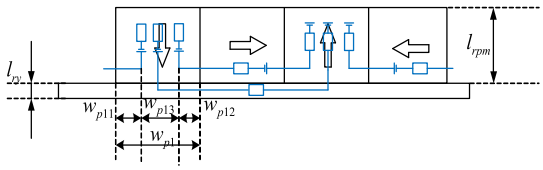


**FIGURE 8.** Magnetic circuit of PM rotor.

are described separately. The circumferentially magnetized rotor PMs are modeled in the same way as the magnetic path of stator PMs. The axially magnetized PMs are divided into three sub PMs, with the two side sub PMs in series with the circumferentially magnetized PMs, the middle sub PMs in series with the rotor yoke [22]. The magnetic circuit of the PM rotor is established as shown in Figure 8.

$$\begin{cases} w_{p11} = w_{p12} = \dfrac{(lry + l_{rpm})^2 - lry^2}{2(lry + l_{rpm})} \\ w_{p13} = w_{rpm} - \dfrac{(lry + l_{rpm})^2 - lry^2}{(lry + l_{rpm})} \\ w_{p1} = w_{rpm} \end{cases} \tag{7}$$

where, $w_{p1}, w_{p11}, w_{p12}, w_{p13}$ are the dimensions shown in Figure 8.

Based on (7), the width of the rotor PM can be calculated, and then it is substituted to (1) and (2) to get magnetomotive force source and the internal magnetic reluctance of rotor PM, and the equivalent magnetic circuit of the PM rotor can be established.

### D. VNMC OF AFFSMGCM

In this paper, the segmentation method is used to model air gap reluctance [12]. In order to simplify the computational difficulties of the VNMC model, the following assumptions are made:

1) The magnetic potential of the surface of stator/rotor pole is equal everywhere.

2) The magnetic flux lines enter or exit perpendicularly to the surface of the iron core.

3) The magnetic field is distributed uniformly along the radial direction and the electromagnetic characteristics are simplified to be calculated at the average radius.

According to the position of the rotor during rotation, the rotor position is divided into several sections (set the position angle of the RMMR tooth as $\theta_i$, and the corresponding position angle of the PM rotor as $\beta_i$), as shown in Figure 9.

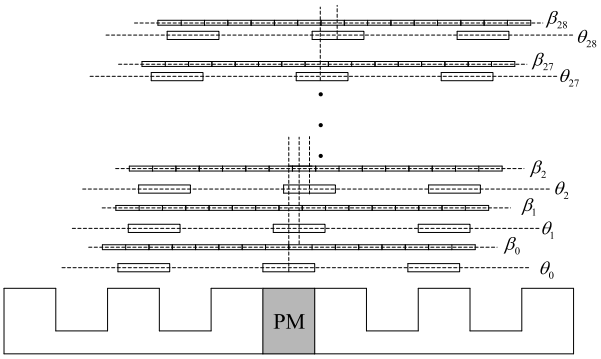


**FIGURE 9.** Rotor position interval division.

By connecting the air gap reluctance with the reluctance of AFFSPMM and PM rotor, the initial position magnetic network of the motor can be established. Then, the corresponding VNMC model can be established according to different rotor position angles. Figure 10 shows 1/6 part of the VNMC model of half AFFSMGCM at the initial position.

The MMF generated by the armature winding at stator yoke can be calculated by

$$F_{wi} = N_w I_i \tag{8}$$

where, $N_w$ and $I_i$ are the number of turns and phase current, respectively.

In this paper, the initial position of the VNMC model is designed at the position as shown in Figure 10(b).

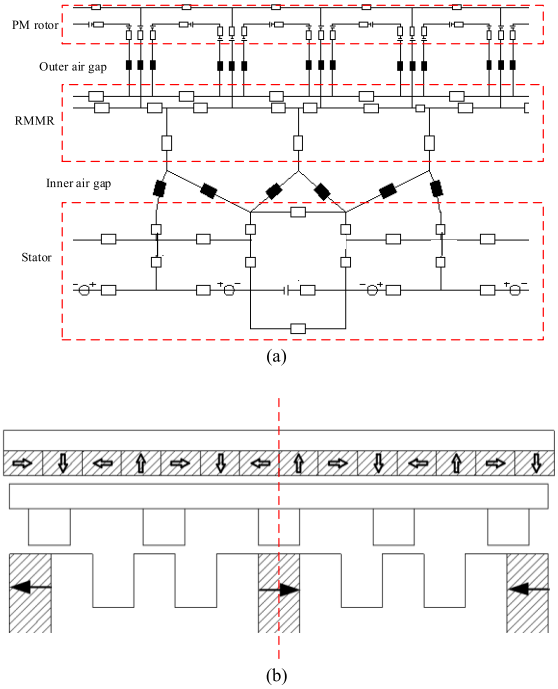


**FIGURE 10.** 1/6 VNMC model of half AFFSMGCM (a) VNMC model. (b) Initial position.

### E. ELECTROMAGNETIC CHARACTERISTIC CALCULATION AND ANALYSIS

When the rotor position changes, although the number of reluctance is various, the total number of nodes in the VNMC model remains constant. Therefore, the solution of the VNMC model can be realized by the node potential equation:

$$\begin{bmatrix} G(1,1) & G(1,2) & \dots & G(1,n) \\ G(2,1) & G(2,2) & \dots & G(2,n) \\ \dots & \dots & \dots & \dots \\ G(n,1) & G(n,2) & \dots & G(n,n) \end{bmatrix} \begin{bmatrix} F_m(1) \\ F_m(2) \\ \dots \\ F_m(n) \end{bmatrix} = \begin{bmatrix} \Phi(1) \\ \Phi(2) \\ \dots \\ \Phi(n) \end{bmatrix} \tag{9}$$

where, $G(i,j)$ is the reluctance branch between the ith node and the jth node, $F_m(i)$ is the MMF of the ith node, and $\Phi(i)$ is the magnetic flux of the ith node. The variables $i$ and $j$ are the number of node, taking an integer value of 1-220.

The permeability $\mu_e$ of the nonlinear reluctance of silicon steel sheet can be calculated by interpolation method. Assuming the calculated flux density $B_e$ is located between two discrete points $P_1(H_{curve}(n), B_{curve}(n))$ and $P_2(H_{curve}(n+1), B_{curve}(n+1))$ of the BH curve as shown in Figure 11, and the calculated permeability is $\mu_e$ by (10). If $\mu_e^{(k+1)}$ and $\mu_e^{(k)}$ meet the error requirement in (11), use the $\mu_e^{(k+1)}$ to calculate the electromagnetic performances and proceed to the next position calculation. Otherwise, $\mu_{new}$ will be updated and $\mu_e$ will be iteratively

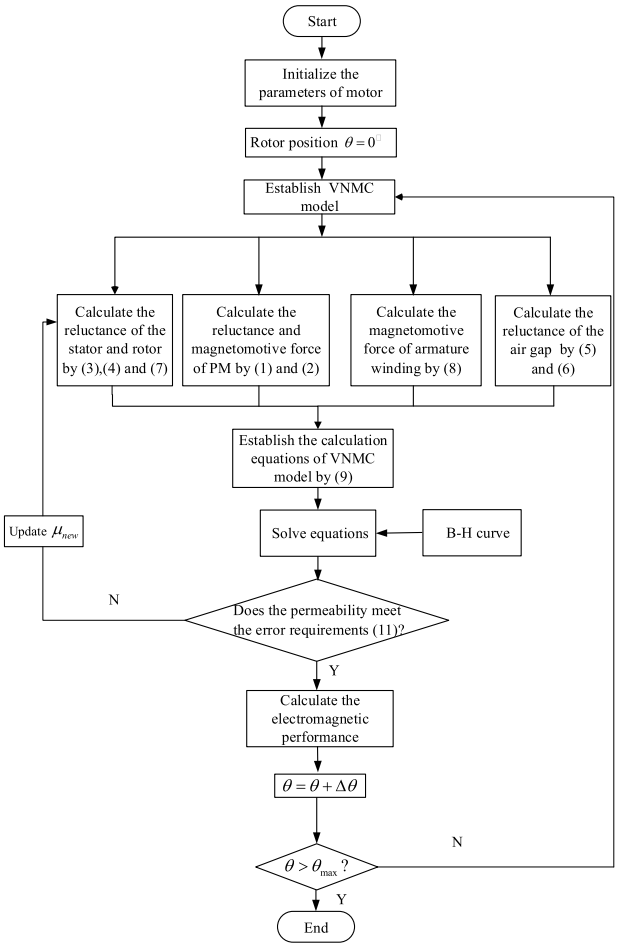


**FIGURE 11.** Calculation flow chart of VNMC model.

calculated again.

$$\begin{cases} H_e = H_{curve}(n) + \frac{(H_{curve}(n+1)-H_{curve}(n))(B_e-B_{curve}(n))}{B_{curve}(n+1)-B_{curve}(n)} \\ \mu_e = \frac{B_e}{H_e} \end{cases} \tag{10}$$

where, $H$ is the coercivity.

$$\max \left| \mu_e^{(k+1)} - \mu_e^{(k)} \right| \leq \zeta_\mu \tag{11}$$

where, $k$ is the number of iteration steps, and $\zeta_\mu$ is the minimum error.

To validate the effectiveness and accuracy of the proposed VNMC model, the calculation results were compared with the FEA results. The VNMC model is solved according to the flow chart in Figure11, and the calculation results compared with the FEA results are shown in Figure 12.

It can be seen from Figure 12 that the calculation results of VNMC method and FEA method are in good agreements, which verifies the correctness of the calculation of VNMC model.

Compare the calculation time of the VNMC model and the FEA model in the case of one electrical cycle in 60 steps, the result shows the FEA model takes 42 minutes, while the VNMC model only takes 2 minutes, which indicates that the proposed VNMC model can greatly reduce the time of calculation.

**TABLE 2.** Parameter Sensitivity analysis of affspmm by vnmc method.

| Symbol | Quantity | $S_T$ | $S_{T_{rip}}$ | $S_c$ |
|---|---|---|---|---|
| $k_{io}$ | Split ratio | -1.52 | 1.91 | 1.72 |
| $w_{spm}$ | Stator PM inner width | -0.65 | -1.02 | 0.84 |
| $l_{mry}$ | Axial length of RMMR yoke | 0.24 | -1.04 | 0.64 |
| $w_{rt}$ | RMMR tooth inner width | -0.08 | 0.17 | 0.13 |
| $g_1$ | Axial length of inner gap | 0.2 | -0.80 | 0.50 |
| $w_{sl}$ | Stator slot inner width | 0.59 | -0.39 | 0.49 |
| $w_{st}$ | Stator tooth inner width | -0.58 | 0.57 | 0.58 |

**TABLE 3.** Parameter Sensitivity analysis of affspmm by fea method.

| Symbol | Quantity | $S_T$ | $S_{T_{rip}}$ | $S_c$ |
|---|---|---|---|---|
| $k_{io}$ | Split ratio | -1.79 | 2.01 | 1.90 |
| $w_{spm}$ | Stator PM inner width | -0.54 | -0.93 | 0.74 |
| $l_{mry}$ | Axial length of RMMR yoke | 0.21 | -1.22 | 0.71 |
| $w_{rt}$ | RMMR tooth inner width | -0.07 | 0.21 | 0.14 |
| $g_1$ | Axial length of inner gap | 0.25 | -0.67 | 0.46 |
| $w_{sl}$ | Stator slot inner width | 0.49 | -0.35 | 0.42 |
| $w_{st}$ | Stator tooth inner width | -0.73 | 0.52 | 0.63 |

## IV. MULTI-OBJECTIVE OPTIMIZATION OF AFFSMGCM BASED ON VNMC METHOD

### A. SENSITIVITY ANALYSIS OF VARIOUS STRUCTURAL PARAMETERS OF AFFSPMM

In order to improve the efficiency of optimization, assuming that the size of the PM rotor is unchanged at first, then the sensitivity of structural parameters of AFFSPMM is analyzed. The sensitivity $S(x)$ is expressed in (12).

$$S(x) = Avg[S(x_i)] = Avg\left[ \frac{\left( \frac{F(x_0 \pm \Delta x_i) - F(x_0)}{F(x_0)} \right)}{\frac{\pm \Delta x_i}{x_0}} \right] \tag{12}$$

where, $x$ is the design parameter; $x_0$ is the initial value of design parameters; $x_i$ is the change value of parameter; $F(x)$ is the target value.

$S_T$ and $S_{T_{rip}}$ is the sensitivity of average output torque and torque ripple, respectively. The comprehensive sensitivity $S_c$ is introduced in (13), and the weight coefficient $\lambda_1$, $\lambda_2$ are set to 0.5:

$$S_c = \lambda_1 |S_T| + \lambda_2 \left| S_{T_{rip}} \right| \tag{13}$$

The sensitivity values and comprehensive sensitivity values of each design parameter are calculated based on VNMC and FEA method, and the results are shown in TABLE 2 and TABLE 3.

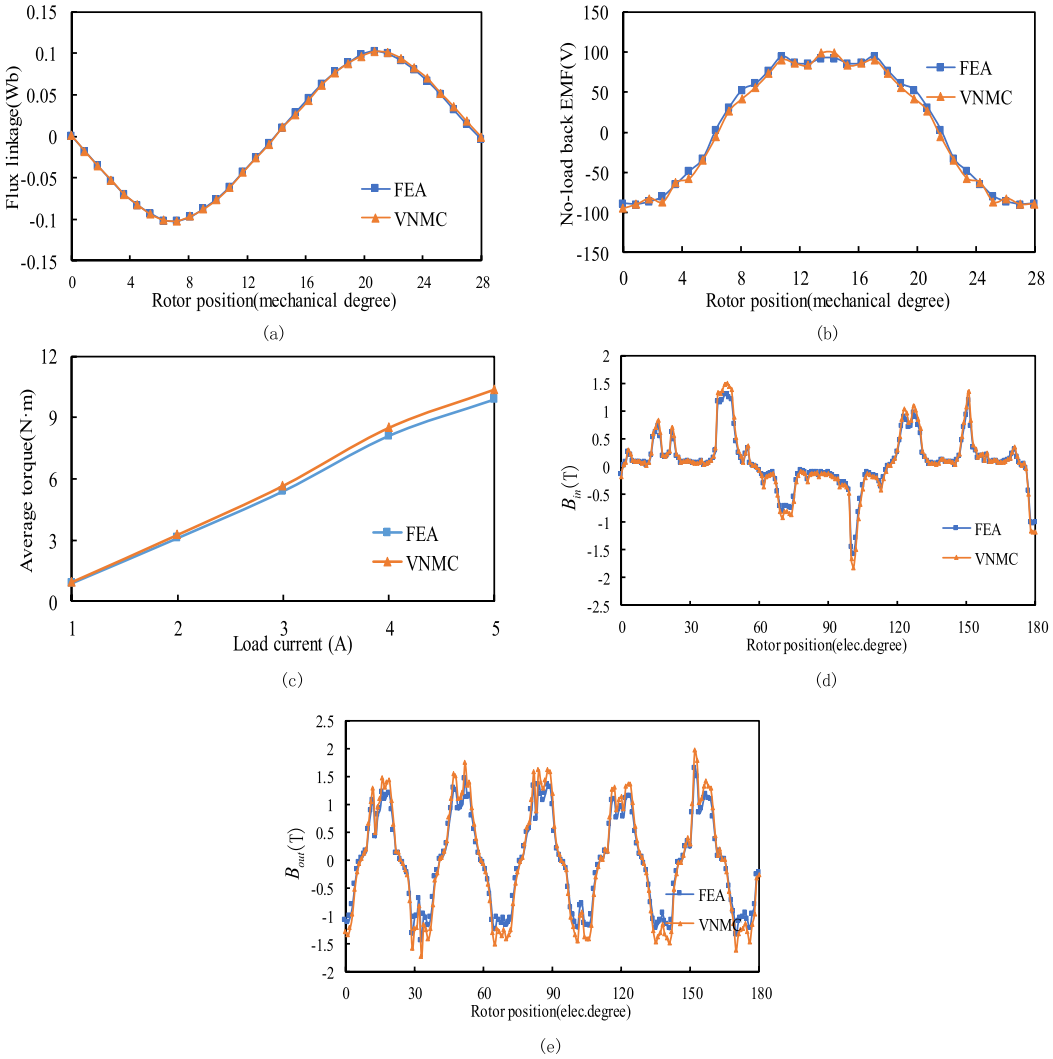


**FIGURE 12.** Comparison of calculation results by VNMC method and FEA method. (a) A-phase no-load flux linkage of AFFSMGCM at 975rpm. (b) A-phase no-load EMF of AFFSMGCM at 975rpm. (c) Output torque of AFFSMGCM at 975rpm. (d) Inner air gap flux density of AFFSMGCM under the rated condition. (e) Outer air gap flux density of AFFSMGCM under the rated condition.

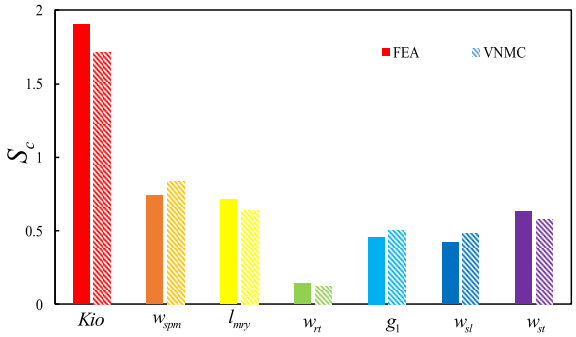


**FIGURE 13.** Comparison of analysis results between VNMC method and FEA method.

Figure13 shows the comparison of analysis results between VNMC method and FEA method.

It shows that although there are errors in the sensitivity calculation values of the parameters obtained by the two methods to the optimization target, the strength is basically the same.

### B. MULTI-OBJECTIVE OPTIMIZATION OF AFFSPMM

The optimization variables are divided into three layers according to (14).

$$Ranges = \begin{cases} Low : S_c \le 0.4 \\ Middling{:}0.4 \le S_c \le 0.7 \\ High : S_c \ge 0.7 \end{cases} \tag{14}$$

It can be seen from TABLE 2 and TABLE 3 that the $k_{io}$, $w_{spm}$ and $l_{mry}$ have a high impact on the optimization objectives, so those are selected as the optimization variables, and keep other parameters unchanged.

The BP neural network algorithm is used to fit the fitting function of highly sensitive variables with respect to the optimization objective by (15).

$$y_i = f(x_1, x_2, x_3) i = 1, 2 \tag{15}$$

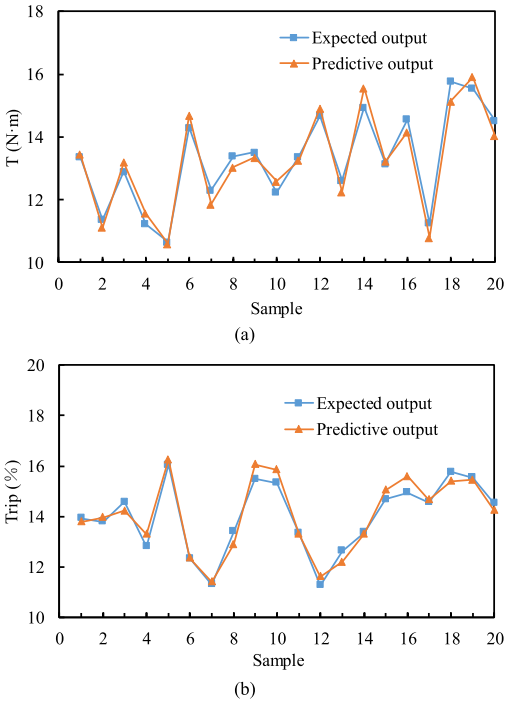


**FIGURE 14.** Fitting results by BP neural network. (a) Fitting results of output torque. (b) Fitting results of torque ripple.

**TABLE 4.** Fitting effect of torque and torque ripple.

| | Output torque | Torque ripple |
|---|---|---|
| R-Squared | 0.953 | 0.942 |

where, $y_i$ is the fitting value of output torque and torque ripple, and $x_1$, $x_2$, $x_3$ is the independent variable $k_{io}$, $w_{spm}$ and $l_{mry}$, respectively.

In this paper, the number of neural networks in the input layer, hidden layer, and output layer of the BP neural network is set to 3,7,2, respectively. The fitting results are shown in Figure 14.

The determination coefficient R-square is introduced to determine the quality of the fitting effect, and the results are shown in TABLE 4.

It can be seen from TABLE 4 that the R-Squared values of both output torque and torque ripple are greater than 0.9, indicating that the fitting model has better fitting accuracy.

Using the fitting results as input of the cuckoo algorithm, the optimization variables are globally optimized based on the cuckoo algorithm to obtain the Pareto optimal solution set, and then the optimal solution is determined. The optimization design flow chart is shown in Figure 15.

Taking large output torque and low torque ripple as optimization objectives, the optimal solution of Pareto solution set is selected according to (16).

$$f(x_i)_{\min} = \lambda_1 \frac{T_0}{T} + \lambda_2 \frac{T_{rip}}{T_{rip0}} \tag{16}$$

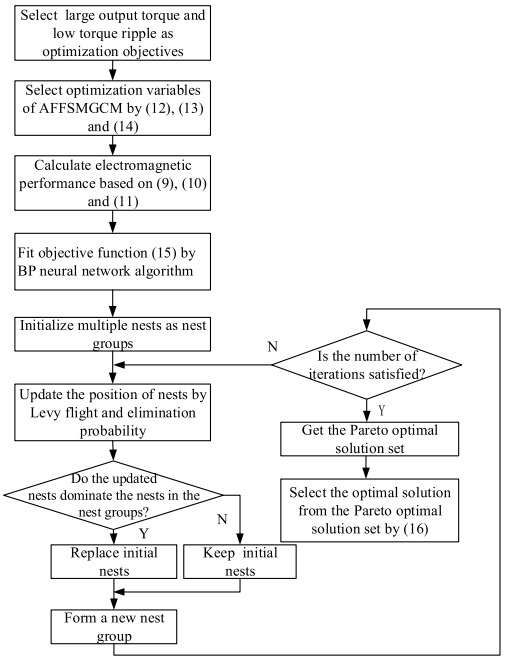


**FIGURE 15.** The optimization design flow chart.

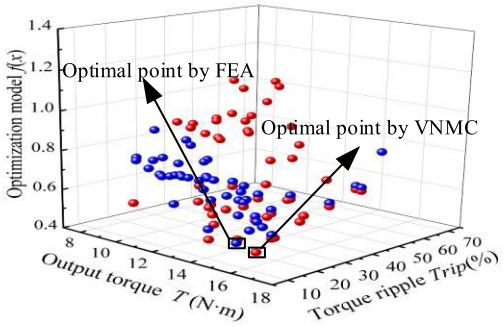


**FIGURE 16.** Pareto optimal solution set.

**TABLE 5.** Items before and after optimization by vnmc method and fea method.

| Items | Initial values | Optimal values by VNMC | Optimal values by FEA |
|---|---|---|---|
| $w_{spm}$ | 10° | 9.86° | 10° |
| $l_{mry}$ | 6 mm | 7.75 mm | 7.6 mm |
| $k_{io}$ | 0.55 | 0.48 | 0.5 |
| $T$ | 10.53 N·m | 15.58 N·m | 14.76 N·m |
| $T_{rip}$ | 17.53% | 16.23% | 15.14% |

where, $T_0$, $T_{rip0}$ are the initial values of output torque and torque ripple.

Figure 16 shows the Pareto optimal solution set by FEA method and VNMC method, and the parameters and performance before and after optimization are shown in TABLE 5.

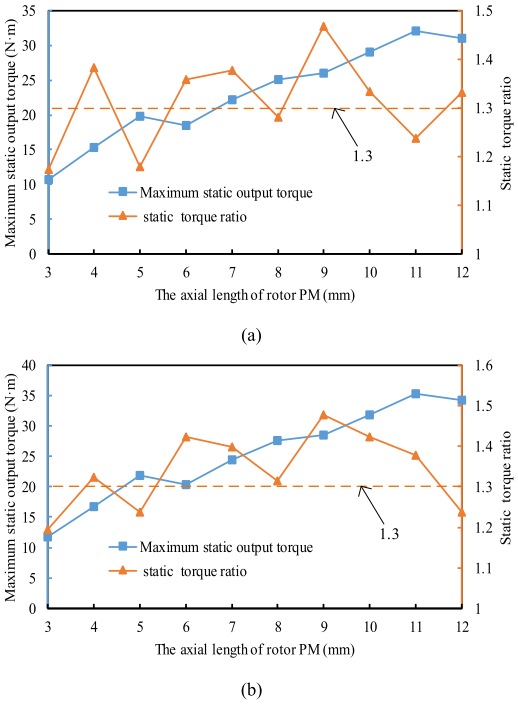


**FIGURE 17.** Effect of axial length of rotor PMs on performance of torque transmission.(a) The results analyzed by FEA method. (b) The results analyzed by VNMC method.

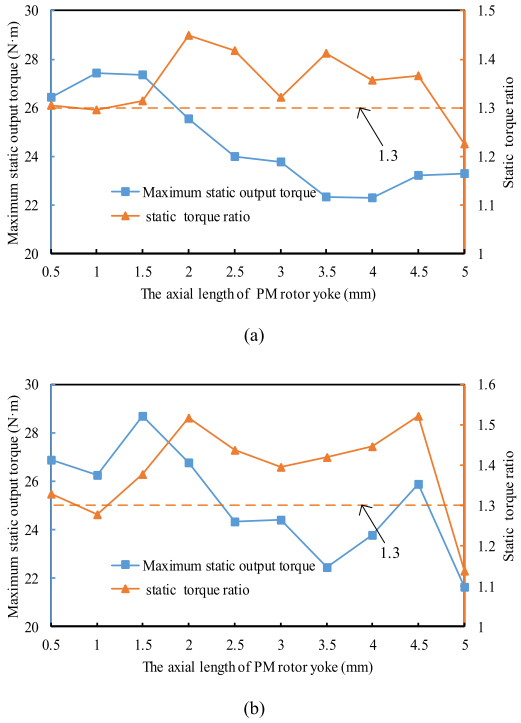


**FIGURE 18.** Effect of axial length of PM rotor yoke on performance of torque transmission.(a) The results analyzed by FEA method. (b) The results analyzed by VNMC method.

As the Table 5 shown, by using VNMC method to optimize the motor, the output torque is increased 47.96% from 10.53N·m to 15.58N·m, and the torque ripple is decreased by 7.42% from 17.53% to 16.23%. The parameters optimized by FEA method and VNMC method are basically in good agreements.

### C. OPTIMIZATION OF PM ROTOR

As the output rotor of the AFFSMGCM, the axial length of the rotor PMs and the yoke of the PM rotor will affect the torque transmission performance. Keeping the optimized parameters of AFFSPMM unchanged and the above variables are optimized furtherly.

Assuming the other parameters remain unchanged, the effects of the axial length of the rotor PMs and PM rotor yoke on the torque transmission performance are studied. The results are shown in Figure 17 and Figure 18.

In order to improve the performance of torque transmission, the static torque ratio should be similar to the theoretical value of the speed ratio 1.3. At the same time, considering the amount and cost of the PMs, the axial length of the rotor PMs are selected as 8 mm as shown in Figure 17.

When the axial length of the rotor yoke is 1mm or 0.5mm, the maximum static torque ratio is closest to 1.3 in Figure 18, but when the length is 0.5mm, the maximum flux density is 2.15T in Figure 19, which means the yoke is oversaturated, and the too thin rotor yoke will also affect the stiffness of PM rotor. Therefore, the thickness of the yoke is determined

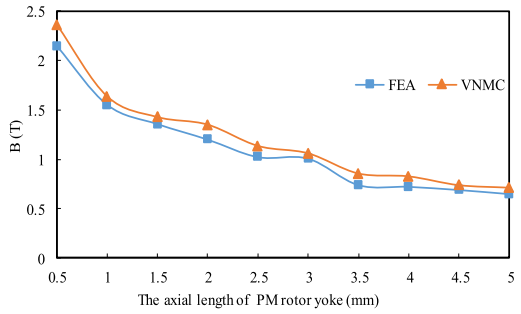


**FIGURE 19.** Maximum flux density in PM rotor yoke with the variation of axial length of PM rotor yoke.

as 1mm. The optimization results of the PM rotor are shown in TABLE 6.

TABLE 6 shows that the maximum static torque is increased by 13.56% from 24.145N·m to 27.420N·m after optimization, and the static torque ratio is closer to the theoretical value of transfer ratio 1.3 in contrast with initial values.

Comparing the performance of AFFSMGCM before and after optimization under the rated condition of 4A, the results are shown in TABLE 7.

It can be seen from TABLE 7 that, the performance of AFFSMGCM have been improved after optimization. The output torque is increased by 32.94% from 8.56N·m to 11.38N·m, the torque ripple is decreased by 26.52% from 12.67% to 9.31%, the torque density is increased by 35.71% from 1.82N·m/L to 2.47N·m/L, the power factor is increased

**TABLE 6. Optimization results of the pm rotor.**

| Items | Initial values | Optimal values |
|---|---|---|
| $R_{lpm}$ | 7 mm | 8 mm |
| $l_{ry}$ | 3 mm | 1 mm |
| Maximum static output torque | 24.145 N·m | 27.420 N·m |
| Static torque ratio | 1.281 | 1.295 |

**TABLE 7. Performance comparison of AFFSMGCM before and after optimization.**

| Performance | Before optimization | After optimization |
|---|---|---|
| Output torque (N·m) | 8. 56 | 11.38 |
| Torque ripple (%) | 12.67 | 9.31 |
| Torque density (N·m/L) | 1. 82 | 2. 47 |
| Power factor | 0.80 | 0.87 |
| Efficiency (%) | 86.94 | 87.83 |

by 8.75%, and the efficiency is increased from 86.94% to 87.83%.

## V. CONCLUSION

The nonlinear VNMC model of the AFFSMGCM is developed in this paper, based on which the multi-parameter and multi-objective optimization of AFFSMGCM is carried out and the optimized results are compared with those by FEA model. It is found that the electromagnetic characteristics calculated by VNMC method are in good agreements with those of the FEA method, but the calculation time of VNMC method only takes up about 5% of the calculation time of the FEA method. The output torque, torque density and efficiency of AFFSMGCM are increased by 32.94%, 35.71%, and 1.02%, respectively. The torque ripple is decreased by 26.52% and the power factor increases from 0.8 to 0.87. The developed VNMC model improves efficiency and accuracy of design and optimization of AFFSMGCM, laying a good foundation for the further development and application of AFFSMGCM.

## REFERENCES

[1] B. Bilgin, B. Howey, A. D. Callegaro, J. Liang, M. Kordic, J. Taylor, and A. Emadi, "Making the case for switched reluctance motors for propulsion applications," *IEEE Trans. Veh. Technol.*, vol. 69, no. 7, pp. 7172–7186, Jul. 2020, doi: 10.1109/TVT.2020.2993725.

[2] B. Zaghari, A. Stuikys, A. S. Weddell, and S. Beeby, "Efficient energy conversion in electrically assisted bicycles using a switched reluctance machine under torque control," *IEEE Access*, vol. 8, pp. 202401–202411, 2020, doi: 10.1109/ACCESS.2020.3036373.

[3] X. Wang, Z. Wan, L. Tang, W. Xu, and M. Zhao, "Electromagnetic performance analysis of an axial flux hybrid excitation motor for HEV drives," *IEEE Trans. Appl. Supercond.*, vol. 31, no. 8, pp. 1–5, Nov. 2021, doi: 10.1109/TASC.2021.3101785.

[4] Z. Q. Zhu, H. Y. Li, R. Deodhar, A. Pride, and T. Sasaki, "Recent developments and comparative study of magnetically geared machines," *CES Trans. Electr. Mach. Syst.*, vol. 2, no. 1, pp. 13–22, Mar. 2018, doi: 10.23919/TEMS.2018.8326448.

[5] R. Wang, W. Zhang, X. Xu, and J. Zhao, "Analysis and research on magnetic modulation mechanism of axial field flux-switching composite machines," *J. Power Electron.*, vol. 23, no. 5, pp. 789–799, May 2023.

[6] L. Cao, K. T. Chau, C. H. T. Lee, and W. Lam, "Design and analysis of a new parallel-hybrid-excited machine with harmonic-shift structure," *IEEE Trans. Ind. Electron.*, vol. 67, no. 3, pp. 1759–1770, Mar. 2020, doi: 10.1109/TIE.2019.2907445.

[7] R. Cao, E. Su, and M. Lu, "Comparative study of permanent magnet assisted linear switched reluctance motor and linear flux switching permanent magnet motor for railway transportation," *IEEE Trans. Appl. Supercond.*, vol. 30, no. 4, pp. 1–5, Jun. 2020, doi: 10.1109/TASC.2020.2965874.

[8] K. S. Amitkumar, R. Thike, and P. Pillay, "Linear amplifier-based power-hardware-in-the-loop emulation of a variable flux machine," *IEEE Trans. Ind. Appl.*, vol. 55, no. 5, pp. 4624–4632, Sep. 2019, doi: 10.1109/TIA.2019.2921286.

[9] W. Qin, G. Lv, and Y. Ma, "Three-dimensional analytical modeling of axial flux permanent magnets maglev motor," *CES Trans. Electr. Mach. Syst.*, vol. 6, no. 4, pp. 438–444, Dec. 2022, doi: 10.30941/CES-TEMS.2022.00055.

[10] N. Ullah, F. Khan, A. Basit, M. Shahzad, A. H. Milyani, and S. Alghamdi, "Experimental validation of computationally efficient lumped parameter thermal model developed for hybrid excited linear flux switching machine," *Ain Shams Eng. J.*, vol. 14, no. 1, Feb. 2023, Art. no. 101836.

[11] M. Cheng, K. T. Chau, C. C. Chan, E. Zhou, and X. Huang, "Nonlinear varying-network magnetic circuit analysis for doubly salient permanent-magnet motors," *IEEE Trans. Magn.*, vol. 36, no. 1, pp. 339–348, Jan. 2000, doi: 10.1109/20.822544.

[12] Z. Q. Zhu, Y. Pang, D. Howe, S. Iwasaki, R. Deodhar, and A. Pride, "Analysis of electromagnetic performance of flux-switching permanent-magnet machines by nonlinear adaptive lumped parameter magnetic circuit model," *IEEE Trans. Magn.*, vol. 41, no. 11, pp. 4277–4287, Nov. 2005, doi: 10.1109/TMAG.2005.854441.

[13] G. Zhang, W. Hua, and M. Cheng, "Nonlinear magnetic network models for flux-switching permanent magnet machines," (in Chinese), *Sci. China Technological Sci.*, vol. 59, no. 3, pp. 494–505, Mar. 2016.

[14] X. Zhu, Y. Jian, Z. Xiang, D. Fan, and M. Yang, "Multi-objective optimisation of a permanent magnet flux-switching motor by combined parameter sensitivities analysis with non-linear varying-network magnetic circuit method," *IET Electr. Power Appl.*, vol. 13, no. 1, pp. 24–30, Jan. 2019.

[15] H. Wang, K. T. Chau, C. H. T. Lee, C. C. Chan, and T. Yang, "Nonlinear varying-network magnetic circuit analysis of consequent-pole permanent-magnet motor for electric vehicles," *World Electr. Vehicle J.*, vol. 12, no. 4, p. 254, Dec. 2021.

[16] J. Cui, W. Xiao, W. Zou, S. Liu, and Q. Liu, "Design optimisation of submersible permanent magnet synchronous motor by combined DOE and Taguchi approach," *IET Electr. Power Appl.*, vol. 14, no. 6, pp. 1060–1066, Jun. 2020.

[17] Z. Shi, X. Sun, G. Lei, Z. Yang, Y. Guo, and J. Zhu, "Analysis and optimization of radial force of permanent-magnet synchronous hub motors," *IEEE Trans. Magn.*, vol. 56, no. 2, pp. 1–4, Feb. 2020, doi: 10.1109/TMAG.2019.2953731.

[18] Y. Li, C. Zhu, L. Wu, and Y. Zheng, "Multi-objective optimal design of high-speed surface-mounted permanent magnet synchronous motor for magnetically levitated flywheel energy storage system," *IEEE Trans. Magn.*, vol. 55, no. 7, pp. 1–8, Jul. 2019, doi: 10.1109/TMAG.2019.2906994.

[19] A. Fatemi, D. M. Ionel, M. Popescu, Y. C. Chong, and N. A. O. Demerdash, "Design optimization of a high torque density spoke-type PM motor for a formula e race drive cycle," *IEEE Trans. Ind. Appl.*, vol. 54, no. 5, pp. 4343–4354, Sep. 2018, doi: 10.1109/TIA.2018.2844804.

[20] S. Zheng, X. Zhu, L. Xu, Z. Xiang, L. Quan, and B. Yu, "Multi-objective optimization design of a multi-permanent-magnet motor considering magnet characteristic variation effects," *IEEE Trans. Ind. Electron.*, vol. 69, no. 4, pp. 3428–3438, Apr. 2022.

[21] C. Xiao, A. Han, W. Xie, and M. He, "Fast design of spoke-type PM motor with auxiliary notches based on lumped-parameter magnetic equivalent circuit model and hybrid multiobjective optimizer," *IEEE Access*, vol. 10, pp. 99421–99434, 2022, doi: 10.1109/ACCESS.2022.3207769.

[22] X. Chen and Z. Q. Zhu, "Analytical determination of optimal split ratio of E-core permanent magnet linear oscillating actuators," in *Proc. IEEE Energy Convers. Congr. Expo.*, San Jose, CA, USA, Sep. 2009, pp. 2100–2107, doi: 10.1109/ECCE.2009.5316556.

**XIAOBIN XU** was born in Suzhou, Jiangsu, China, in 1997. He received the B.Sc. degree in building electricity and intelligence from Nantong University, Nantong, China, in 2019, where he is currently pursuing the M.Sc. degree in control science and engineering.

His current research interest includes design and optimization of permanent magnet machine.

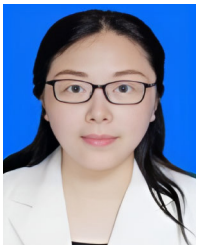

**WEI ZHANG** (Member, IEEE) was born in Taizhou, Jiangsu, China, in 1977. She received the B.Sc. degree in electrical engineering from Nantong University, Nantong, China, in 2000, and the M.Sc. and Ph.D. degrees in electrical engineering from Southeast University, Nanjing, China, in 2007 and 2016, respectively.

From January 2017 to December 2017, she was a Visiting Scholar with The University of Sheffield, Sheffield, U.K. Her current research interests include design and control of permanent magnet brushless machines and drives for automotive applications.

**JINRU CHENG** was born in Changzhi, Shanxi, China, in 2000. She received the B.Sc. degree in electronic information engineering from Nantong University, Nantong, China, in 2022, where she is currently pursuing the M.Sc. degree in control science and engineering.

Her current research interest includes design and optimization of permanent magnet machine.

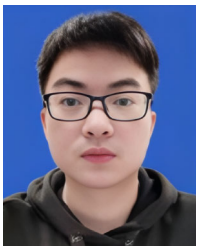

**JIANWEI ZHAO** was born in Bozhou, Anhui, China, in 1996. He received the B.Sc. degree in electrical engineering and automation from the Anhui University of Science and Technology, Bengbu, China, in 2020. He is currently pursuing the M.Sc. degree in control science and engineering with Nantong University, Nantong, China.

His current research interest includes design and optimization of motors.

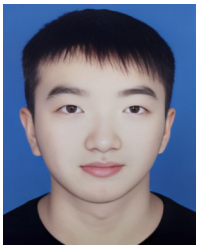

**FENG QIAN** was born in Nantong, Jiangsu, China, in 1998. He received the bachelor's degree in automation from the Chengxian College, Southeast University, in 2020. He is currently pursuing the master's degree in electronic information with Nantong University.

His current research interest includes transformer design and optimization.